Structural variability of edge dislocations in a $SrTiO_3$ low-angle [001] tilt grain boundary

James P. Buban[a)]
Department of Molecular and Cellular Biology, University of California–Davis, Davis, California 95616

Miaofang Chi
Institute of Geophysics and Planetary Physics, Lawrence Livermore National Laboratory, Livermore, California 94550; and Department of Chemical Engineering and Materials Science, University of California–Davis, Davis, California 95616

Daniel J. Masiel
Department of Chemical Engineering and Materials Science, University of California–Davis, Davis, California 95616

John P. Bradley
Institute of Geophysics and Planetary Physics, Lawrence Livermore National Laboratory, Livermore, California 94550

Bin Jiang
FEI Company, Hillsboro, Oregon 97124

Henning Stahlberg
Department of Molecular and Cellular Biology, University of California–Davis, Davis, California 95616

Nigel D. Browning
Department of Chemical Engineering and Materials Science, University of California–Davis, Davis, California 95616; and Condensed Matter and Materials Science Division, Physical and Life Sciences Directorate, Lawrence Livermore National Laboratory, Livermore, California 94550

(Received 31 October 2008; accepted 25 March 2009)

Using a spherical aberration (Cs)-corrected scanning transmission electron microscopy (STEM) and electron energy-loss spectroscopy (EELS), we investigated a 6° low-angle [001] tilt grain boundary in $SrTiO_3$. The enhanced spatial resolution of the aberration corrector leads to the observation of a number of structural variations in the edge dislocations along the grain boundary that neither resemble the standard edge dislocations nor partial dislocations for $SrTiO_3$. Although there appear to be many variants in the structure that can be interpreted as compositional effects, three main classes of core structure are found to be prominent. From EELS analysis, these classifications seem to be related to Sr deficiencies, with the final variety of the cores being consistent with an embedded TiO_x rocksalt-like structure.

I. INTRODUCTION

Grain boundaries have long been known to have far-reaching effects on the bulk properties of perovskite materials. Notable examples include the reduction of the critical currents in high-temperature superconductors ($YBa_2Cu_3O_7$),[1,2] enhancement of the magneto-resistance effect in the manganates ($La_{1-x}Ca_xMnO_3$, $SrCaMnO_3$, etc.),[3,4] and increases in the dielectric constant in $BaTiO_3$ and $SrTiO_3$.[5] For perovskites, the deviation of the grain boundary atomic structure with respect to the bulk typically induces a grain boundary potential, through which the bulk properties are influenced. Accurate calculations of the boundary potentials are extremely advantageous to current materials, and thus a clear understanding of the atomic arrangements at dislocation cores, the key building blocks of grain boundaries, is essential. In addition, recent studies on grain boundary impurity doping in oxides reveal that the atomic arrangement of the cores has a strong influence on the impurity

[a)]Address all correspondence to this author.
e-mail: jpbuban@ucdavis.edu
This paper was selected as an Outstanding Symposium Paper for the 2008 MRS Spring Meeting, Symposium Z. To maintain *JMR*'s rigorous, unbiased peer review standards, the *JMR* Principal Editor and reviewers were not made aware of the paper's designation as Outstanding Symposium Paper.
DOI: 10.1557/JMR.2009.0259

segregation site.[6–8] Therefore, knowledge of the dislocation structure is a necessary component for understanding the mechanics of grain boundary doping—a powerful method to alter or control the influence of the grain boundary on the bulk properties.

Due to its stability and relatively simple structure, grain boundaries in $SrTiO_3$ have long been studied and characterized to serve as a general model for grain boundaries in perovskites.[9–20] Of these reports, the atomic structures of tilt grain boundaries are the most studied. The tilt grain boundary geometry allows a clear projection onto a 2-dimensional plane, making them very suitable for characterization by (scanning) transmission electron microscopy (STEM/TEM). Tilt grain boundaries are usually classified into low-angle or high-angle types. The atomic structure of the former can be described as an array of edge dislocations with a spacing given by Frank's rule, and that of the latter can be described as a small set of structural units.[14] It follows that, for low-angle grain boundaries, if the atomic structures of the edge dislocations are known, then the structure of the grain boundary can be fully understood.

Until now, it has been thought that the general structures of edge dislocations in $SrTiO_3$ (i.e., models for edge dislocations in perovskites in general) have been well defined. In particular, [100] edge dislocations, which comprise the well characterized [001] tilt boundaries, had only been observed to exist as two complementary types,[18,21] often referred to as Sr-rich and Ti-rich. The atomic structures for these two types are illustrated in Fig. 1. The former has a double column of Sr atoms in the center of the dislocation that is thought to be a 2×1 reconstruction of a single column of Sr (a partial or half occupancy), whereas the latter has a double Ti-O column in the core center that is believed to have full Ti site occupancy, but only alternating O sites are occupied in each of the two columns.[9] For simplicity, we will refer to each case as a (columnar) doublet.

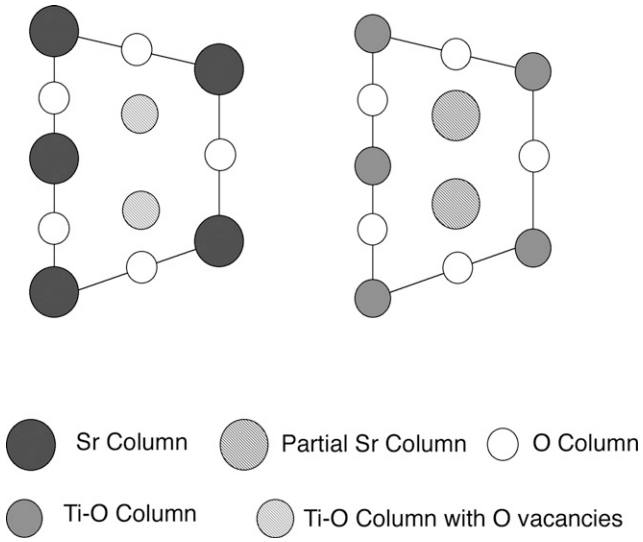

FIG. 1. Standard structure of [100] edge dislocations in $SrTiO_3$. There are two types–Sr-rich (left) and Ti-rich (left).

With the recent advance of spherical aberration (Cs)-corrected STEM, it is now possible to obtain experimental images with higher resolution and better signal-to-noise ratios, as well as electron energy loss spectra (EELS) localized even to single atomic columns.[22] In this manuscript, we report that the high level of detail obtainable with Cs correction reveals that the atomic structure of [001] edge dislocations in $SrTiO_3$ is more complex than was previously thought. We show images exhibiting these variations, give an interpretation of these structural variations by using results from statistical analysis, and discuss the origin of the complexity now apparent in the dislocation structure.

II. EXPERIMENT

A $SrTiO_3$ bicrystal containing a symmetric 6° [001] tilt grain boundary was purchased from Crystec. The TEM specimen was made by cutting a thin slab from the bicrystal with a diamond saw, which was then mechanically polished and thinned by ion milling to electron transparency. Observation of the grain boundary was performed using the FEI 80-300kV Titan at Lawrence Livermore National Laboratory, equipped with both probe and image CEOS correctors, a Tridiem Gatan Imaging Filter HREELS spectrometer, and an EDAX Si(Li) solid-state energy-dispersive x-ray detector. All images and EELS analyses shown here are acquired in STEM mode with the same microscope configuration, i.e., with the same camera length, gun lens, spot size, etc. This process means that no additional beam adjustment is needed and simultaneous imaging and chemical analysis can be achieved. The beam convergent semiangle is 16.8 mrad, the inner HAADF collection angle is 94.9 mrad, and each EELS spectrum was obtained with a single acquisition time of 2.5 s with a collection angle of 9.35 mrad. To avoid excessive beam damage to the beam-sensitive dislocation cores, single atomic column EELS was not conducted. In our work, the EELS acquisition is performed by using a 0.2 nm $\times$ 0.2 nm square scanned on the target area, in which case we are also able to track the atomic column position manually to compensate for the shift caused by beam illumination and the specimen drift. Energy-dispersive x-ray spectroscopy (EDS) was performed by using a beam diameter of 0.3 nm and an acquisition time of 2 s to minimize the irradiation damage.

To better classify the large number of different dislocation core structures, we performed a basic statistical analysis. STEM images of multiple cores were roughly rotated and magnified. They were then cropped to produce

a stack of individual dislocation core images. Each image was then registered to the average of all the images by performing an exhaustive search of the best cross-correlation value resulting from combinations of rotation (±5°), shear (±5°), and magnification (±10%). To generate the atomic column probability density, a peak search was performed on each of the registered images. This was done by performing a normalized cross-correlation of each image with an average Ti atom. A 2-dimensional peak search was then performed on the resulting cross-correlation map, and for each peak location the corresponding pixel in the probability density map is incremented by 1. After this process was performed for each image, the final probability density map was then smoothed by kernel convolution with a 2-dimensional Gaussian (sigma = 1 pixel) curve.

III. RESULTS

A. Z-contrast images

Figure 2 shows a typical high-resolution Z-contrast image of the 3°/3° symmetric [001] tilt grain boundary in $SrTiO_3$. The bright spots in the image correspond to Sr-O columns, whereas the less bright ones are the TiO_2 columns. The dislocation cores are visible as the darker areas in the images, which mainly results from a lower atomic number density, an increased interatomic spacing, and/or a possible dechanneling effect from the strain and orientation effect. The spacing between the cores was determined to be 3.7 nm, and the misorientation angle was measured at 6.0 ± 0.5°, which is consistent with Frank's rule.[23] In addition to the standard types of dislocations commonly observed in $SrTiO_3$ (illustrated schematically in Fig. 1), we found a large variety of additional types of dislocation cores. Several variations were observed, but we focus here on the analysis of the three dislocation core types that were more commonly observed. These three types of core structures will be referred to as elongated, composite, and transformed.

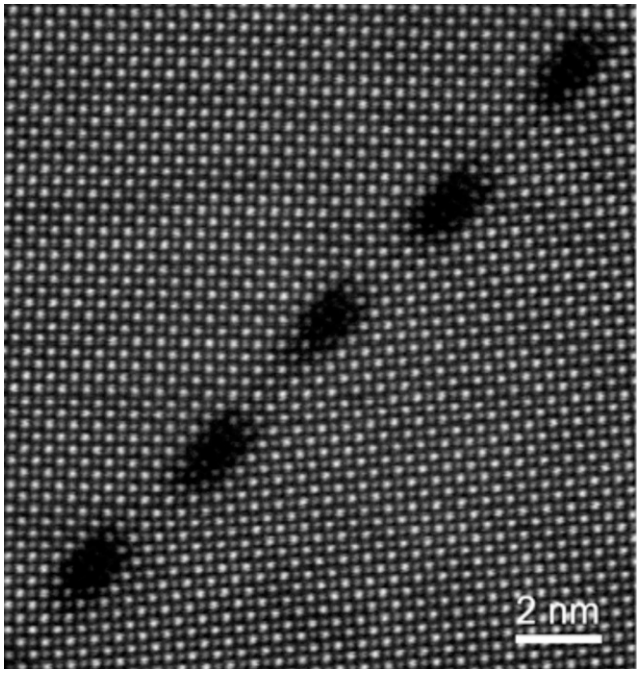

FIG. 2. High-resolution Z-contrast STEM image of the 6° [001] tilt grain boundary in the $SrTiO_3$ bicrystal. The grain boundary is mainly composed of an array of dislocations.

An example of an elongated dislocation core is shown in Fig. 3. Analogous to the standard cores, there are two types of elongated core structures—Ti rich and Sr rich. Compared with the standard core (in Fig. 1), there

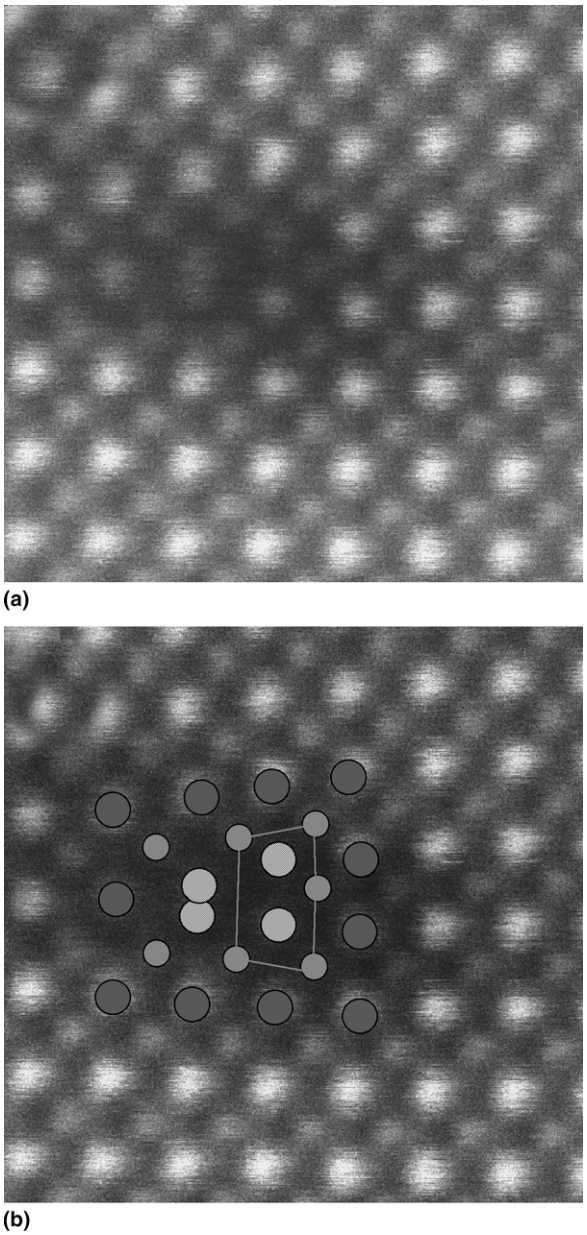

FIG. 3. (a) Z-contrast image of the elongated dislocation core; (b) same image with a structural overlay.

appears to be a splitting of the atomic column along the grain boundary plane immediately adjacent to the typical column doublet seen in the standard core structure. The location and image intensity of these split columns are consistent with a chemical composition similar to the double columns in the center of the core of either type. Apart from this key feature, there is little difference between the elongated core and that of the two standard types. In both elongated and standard cores, the (100) lattice plane terminates on the compressed edge of the dislocation.

As shown in Fig. 4, the composite dislocation core has a more complicated structure. The size of the core region is also longer than the standard and the elongated types; however, the (100) lattice plane terminates at two different locations, corresponding to the two sublattice planes. In turn, we have doublets of both Sr columns and Ti-O columns. This effect is reminiscent of a dissociated dislocation, but there is no observable stacking fault, a characteristic of dissociated dislocations.[17]

The transformed dislocation core structure was the most unexpected [Fig. 5(a)]. Note that, whereas the standard core structures, as well as the elongated and composite structures, exhibit doublets of atomic column of similar image intensity, the transformed cores [Fig. 5(a)] contain two sets of triplets. This effect results in an atomic columnar arrangement considerably different than any previously reported dislocation structures for $SrTiO_3$. The intensity of the triplet columns is commensurate with the intensity of Ti columns, and all transformed

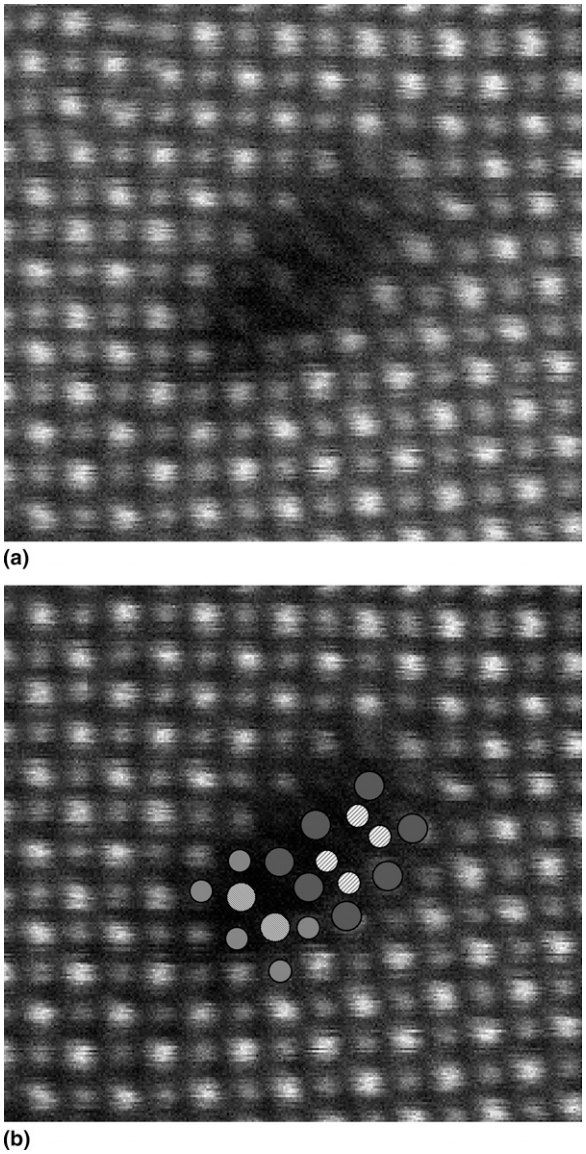

FIG. 4. (a) Z-contrast image of the composite dislocation core; (b) same image with a structural overlay.

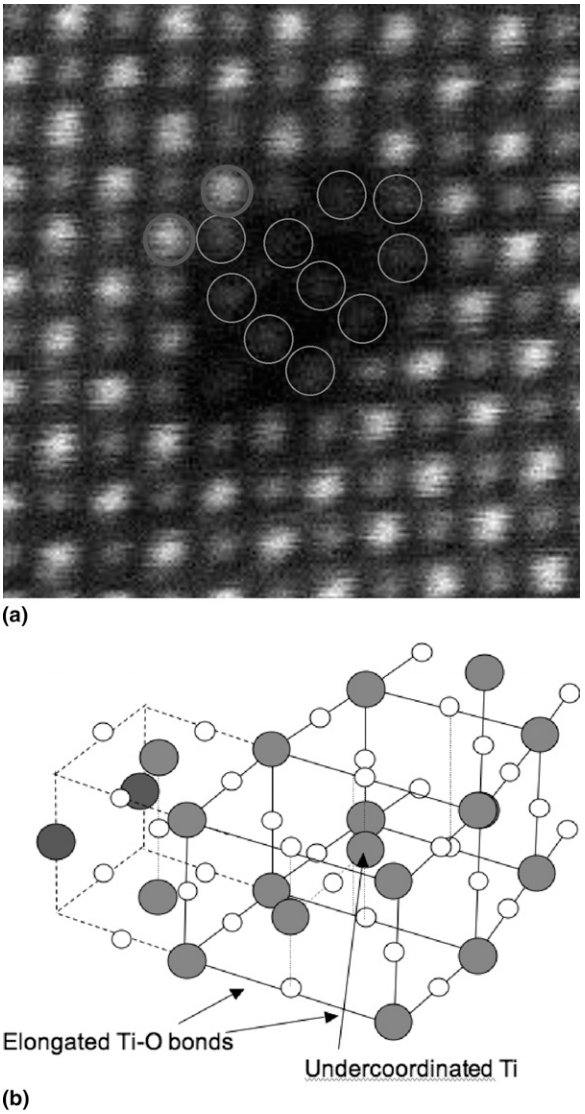

FIG. 5. (a) Z-contrast image of the transformed dislocation; (b) schematic of the transformed dislocation structure.

dislocation cores terminated at the same (100) sublattice plane. There are also a number of columns of weak intensity, which are similar in intensity to the background in the bulk, suggesting that these are columns of oxygen. The length of the transformed core is similar to that of the composite core. We note that the majority of the grain boundary cores observed in this study were of the transformed type.

To illustrate the range of variability in the core structures, we calculated a probability density map [Fig. 6(a)]. Although not all cores are of the same size, the general core region is outlined in the figure to aid the eye. From the plot it can be seen that much of the core region is diffuse, indicating that many different competing sites may be occupied at any given time. An average image of 167 dislocation cores is shown in Fig. 6(b), which is compared with the average image of the elongated, composite, and transformed cores [Fig. 6(c)]. The two averaged images are seen to be similar, giving direct evidence that although there are minor variations along each core, these three structural classifications are prevalent.

B. Electron energy loss and energy-dispersive x-ray spectroscopy

A typical EEL spectrum taken from a region with a high density of transformed dislocations is compared with an EEL spectrum of bulk $SrTiO_3$ in Fig. 7. The raw spectra are shown in Fig. 7(a), whereas the background removed Ti-L and O-K edges are shown in Figs. 7(b) and 7(c), respectively. The Ti-L edges from the bulk exhibit a characteristic splitting of the individual L edges, which is attributed to the spin-orbit coupling of t_{2g} and e_g molecular orbitals of Ti and O ions, and it is $\sim$2.2 eV for the octahedrally coordinated Ti and O in bulk $SrTiO_3$. The e_g peak of Ti-L_3 edge is at $\sim$459.2 eV, whereas the e_g peak of the Ti-L_2 edge is at $\sim$464.7 eV. The O-K edge from the bulk contains four distinct peaks in the near edge fine structure (labeled a–d). Figure 8 shows EDS data acquired from a transformed dislocation and the bulk. The Sr/Ti ratio is significantly reduced at the dislocation core in comparison with the bulk.

The spectrum from the dislocation core reveals several differences in the comparison to the bulk spectrum. The onsets of L_3 and L_2 e_g peaks are shifted (0.5 ± 0.05) eV lower in the dislocation spectra. No obvious shift on the t_{2g} peaks was observed, as a result, the splitting between e_g and t_{2g} in the dislocation spectra is reduced to $\sim$1.3 eV. In addition, the ratio of the total signal in the O-K edge to the total signal in the Ti-L edges is lower at the boundary than in the bulk, indicating a lower O/Ti ratio in the core. Finally, peak b in the O-K edge is almost absent on the core spectra.

In addition, to test the effect of beam damage, we acquired a series of images and spectra with the beam

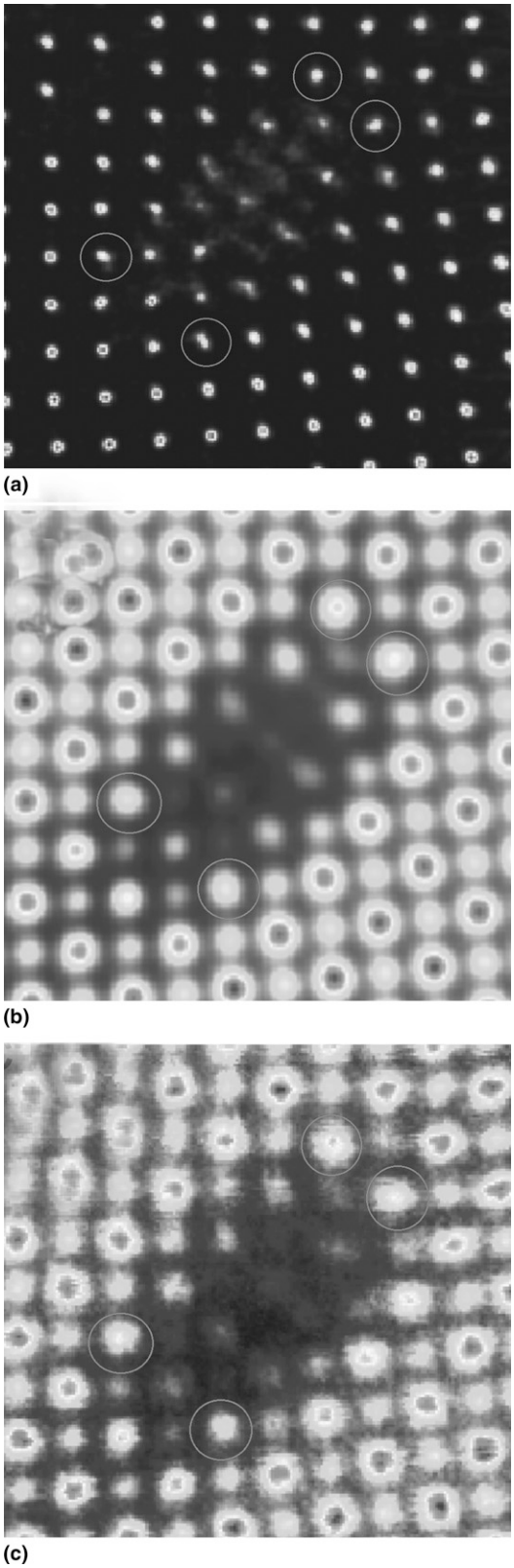

FIG. 6. (a) Probability density plot of column positions for the dislocation cores. The diffuse regions represent areas of large variation: (b) average image of 167 cores; (c) average image of the elongated, composite, and transformed cores. To aid the eye, four corresponding column positions are circled in all three figures.

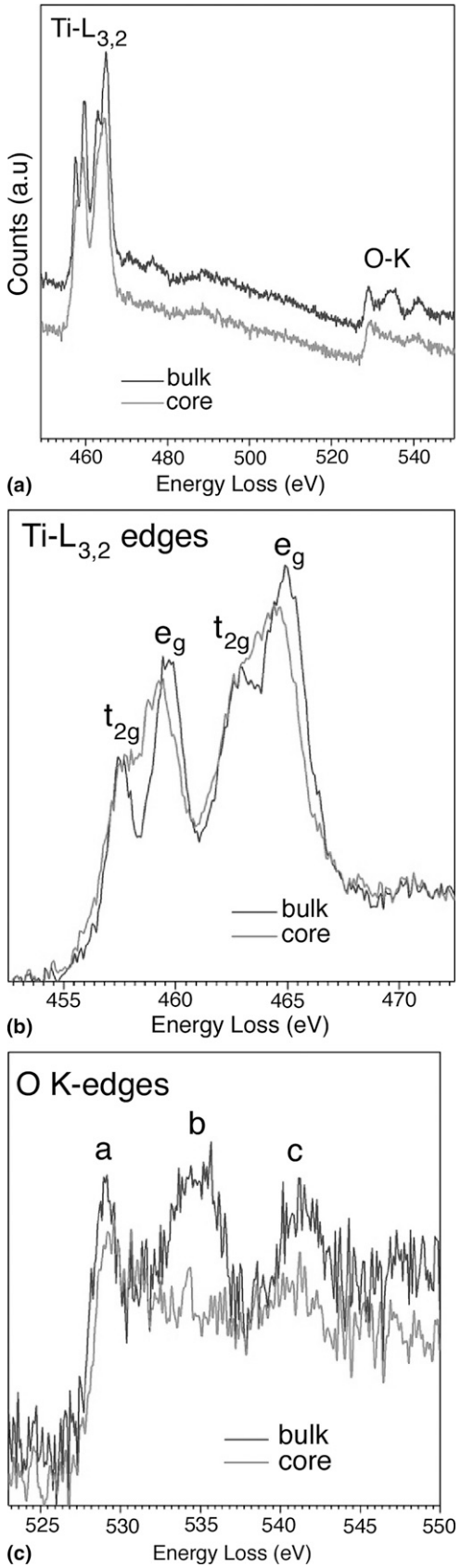

FIG. 7. (a) EEL spectra from the dislocation core and bulk; (b) Ti-L edge of core and bulk; (c) O-K edge of core and bulk.

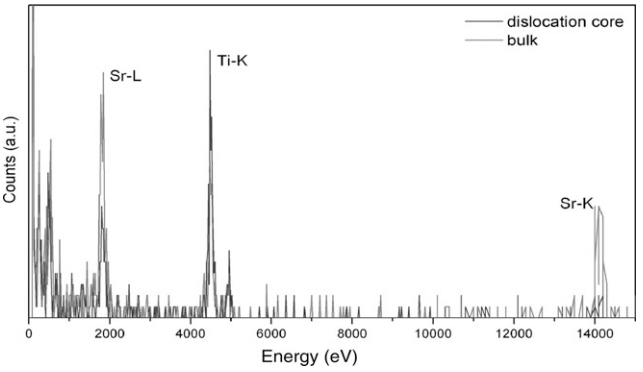

FIG. 8. Energy-dispersive x-ray spectra (EDS) taken from the transformed dislocation and the bulk. The amount of Ti and Sr respectively increase and decrease at the dislocation substantially, in comparison with the bulk.

continuously scanning up to 20 min. The overall atomic arrangement remains the same, with the exception of some slight shifts in the center of the dislocation core. No changes were observed on the fine structures of Ti-L and O-K edges. This result indicates that the beam damage is not the reason for the spectral differences.

IV. DISCUSSION

The structures of the elongated and composite dislocations can be understood by considering the effect of strain at the low misorientation angle. Geometrically, the unit cells in the tensile region of the grain boundary, near the termination of the (100) plane, are expanded considerably in comparison with the unit cells in the bulk. This tensile strain most likely induces a 2×1 reconstruction in the unit cell along the grain boundary plane in the elongated dislocation, as well as a 2×1 reconstruction of slightly off the grain boundary plane in the composite dislocation. With this function in mind, we constructed schematics of the elongated and composite cores, shown in Figs. 5 and 6, respectively. Because of the large difference in the average atomic number of the Sr and Ti-O oxide columns, the determination of the chemical composition is straightforward apart from the reconstructed columns, where a reduction of intensity is expected due to the lower atomic density. In this case, we use to the position of the reconstructed columns with respect to the sublattice to justify our model.

In the elongated core, the extra Sr column doublet is suggestive of a stacking fault type structure, whereas the two different lattice plane termination points are reminiscent of partial dislocations. Although both features are found in dissociated dislocations, neither core type has the partial dislocations or the stacking fault structure that is typical of dislocation dissociation. Instead, it would appear that these dislocations are more of a transitional state. One could imagine that a reduction in the misorientation angle could further cause both the cores

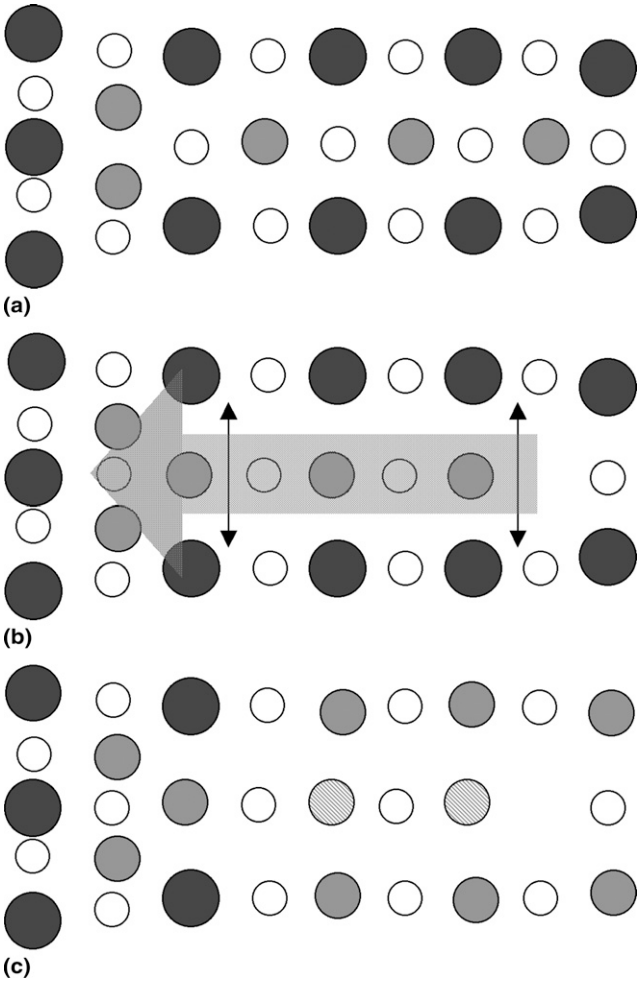

FIG. 9. Model for the transition of a standard dislocation core to a composite core structure. (a) An extended schematic of the Ti-rich dislocation core. (b) The same core with tensile strain applied perpendicular to the grain boundary plane (indicated by black arrows). The central row of atoms has been shifted to the left (indicated by arrow). (c) Six of the Sr columns on either side of the grain boundary plane are now substituted with Ti-O columns.

to elongate and eventually form typical dissociated dislocations. Finally, it is not clear why the 2×1 reconstruction is not always along the grain boundary plane. It has been suggested that intrinsic variations of dislocations may be necessary to mitigate the overall strain of the grain boundary. Indeed, the failure of a "one-size fits all" approach to tilt grain boundaries as an array of dislocations of only two types of dislocations may not seem too surprising.

The intensity of the column triplets in the transformed cores tends to be uniform and is close to that of the Ti-O columns in the bulk, although they lie on the Sr sublattice. We resolve this conflict by considering the coordination, charge, and strain. If the column triplets were composed of Sr, then, from the image intensity, they would probably be partially occupied. This possibility would result in effective Sr vacancies, which, due to charge balance, would induce compensating oxygen vacancies. This effect in turn would reduce the coordination of neighboring Ti ions, causing the Ti to move closer towards the O ions in the bulk.[24] The end result would yield a dislocation core structure that has several vacancies and is highly strained—more so than a standard dislocation core. Moreover, virtually no ion would be fully coordinated within the core structure.

Alternatively, we propose a structure with the triplet columns being composed of Ti-O columns, with the middle column shifted by ½ (001) relative to the other Ti-O columns. This shift gives a local structure reminiscent of that of rocksalt. The chemical composition here is consistent with the intensity in the Z-contrast image. Furthermore, the coordination of nearly all ions is consistent with bulk $SrTiO_3$. Only Ti in one column is under coordinated from 6-fold to 5-fold, and the number of strained bonds is significantly less than the structure with partially occupied Sr columns described above. The longest bonds, which are between Ti and O ions, are no more strained than those found in the standard Ti-rich dislocations.

The Ti-O triplets are also more consistent with the EELS results than columns of partially occupied Sr. Energy shifts in the Ti-L edge indicate a reduction of the Ti oxidation state from 4+ in bulk $SrTiO_3$.[25] This result is consistent with the under coordination of the Ti in the central column as well as an elongation of the Ti-O bonds. A similar energy shift has also been observed in other studies on $SrTiO_3$ dislocation cores.[16,20] Furthermore, the decrease of the splitting between e_g and t_{2g} peaks in the dislocation spectra is indicative of a reduction of crystal-field splitting, implying a change in Ti-O coordination at the grain boundary via a change in the number of the nearest oxygen neighbors and/or the Ti-O bond lengths. For the O-K edge, the most notable feature is the disappearance of peak c. Reduction in peak c can been linked to Sr vacancies because this peak mainly arises from interactions of O^{2-} ions with Sr^{2+} ions.[26–29] In this case, the virtual absence of peak B indicates a (near) complete depletion of Sr in the transformed dislocation cores, resulting in a structure composed of Ti and O ions only. A further comparison of the O-K edge to those of binary titanium oxides from the studies by Mitterbauer[30] reveals that the O-K fine structure of the dislocation core is similar to TiO, where the t_{2g} and e_g splitting is hardly visible and the ratio of peak B to A is lower compared with TiO_2 or Ti_2O_3. Upon depletion of Sr, the Ti and O atoms at the boundary probably relax and change the octahedron bonding from corner-sharing to edge-sharing. As a result, the atomic arrangement in the core is a rocksalt-like structure, similar to TiO.

It is necessary to confirm viability of the transformed structure with calculations. However, using the current model, we speculate that the transformed core contains a nanocolumn of TiO_x imbedded in the $SrTiO_3$ matrix.

More recently, grain boundary doping mechanisms have been shown to be strain-driven and substitute to specific pre-existing lattice sites.[6–8] Here, it appears that Ti-O columns substitute for pre-existing Sr column sites. In a sense this may be a sort of "self-doping," which with further study could give insight into additional mechanisms for grain boundary doping.

A second look at the three new variations may also allow some speculation that the different cores may be able to transmute under the right conditions. In fact, the large number of variations observed in the Z-contrast images may be a result of transitionary structures between the three main variants. For example, a comparison of the elongated core with the composite core shows that the main difference is an additional splitting of two Ti-O columns along the grain boundary. Because the tensile strain perpendicular to the grain boundary plane is large in all types of cores, it is possible that the elongated core can transform into the composite core with just a small addition of tensile strain, allowing the Ti-O columns to reconstruct. Likewise, the additional tensile strain may cause a standard Ti-rich core to convert into a transformed core. This process can be imagined by first allowing the lattice to expand perpendicular to the boundary plane. With the extra space available, the first three pairs of Ti-O and O columns on the boundary plane slide by half a unit cell toward the original core location. Finally, the Sr columns on either side of the shifted columns are replaced by Ti-O columns. The process is illustrated schematically in Fig. 8. A local Ti excess at the grain boundary plane may be an additional prerequisite for such a transition to occur. A study of the dislocation core energetics from first principles should be able to give more insight to the validity of these proposed mechanisms.

The above discussion mainly relies on the assumption that strain due to the misorientation of the grains is not fully alleviated by the standard dislocation core structure, and, therefore, small residual strain remains locally at many of the dislocations, which drives structural deviations from the standard dislocation core structure. An alternative to strain being the basis for the structural variations is that small chemical variations along the interface cause the differences in the structures. Despite significant structural variations, the dislocation cores exhibit a uniform spacing along the grain boundary plane. This effect suggests that the energy differences due to strain between the cores (i.e., the strain) cannot be large, which opens the possibility that the observed structural variations require a different driving force. Chemical variations at the interface may provide this force through local nonstoichiometry, which can cause charge imbalances or the excess of ions having bond-lengths incommensurate with the available lattice sites. The latter would induce chemically driven strain, in contrast to the geometric strain at the boundary caused by the misorientation of the two grains. The actual cause of the large variety of dislocation structures observed in this study is most likely the result of the interplay between the local strain and chemical differences along the grain boundary.

Indeed, the alternating half unit cell shifts that are sometimes observed in perovskite grain boundaries may be a simple example of the interaction between local chemical and strain variations. For example in both high- and low-angle grain boundaries in $SrTiO_3$, dislocations have been observed to line up in a straight line along the grain boundary plane as well as being shifted by ½ of a unit cell perpendicular to the grain boundary plane in an alternating fashion.[14,20,21] In the former case, the cores alternate between Sr-rich and Ti-rich, whereas in the latter case all cores will be either Sr-rich or Ti-rich. Here, one can note that the local strain fields will be different depending on whether all cores are in-line or whether they are shifted.

Because every image obtained from a STEM is a projection of a 3-dimensional structure, we address the possibility that the apparent new variations in the dislocation structure are actually the result of imaging dislocation cores that have kinks along the direction perpendicular to the image plane. In general, a kink in which the emission of the dislocation is shifted by only one unit cell should be the most energetically favorable because the energy should increase as the total length of the dislocation increases. Therefore, if a standard dislocation kinked in such a manner, then a projection of the structure along the dislocation direction would show a structure that is disordered over two unit cells. Only the elongated core shows disordering confined to two unit cells. However, apart from the additional splitting of a single atomic column in the grain boundary plane, the elongated core is virtually identical to the standard core structure. A projection of two standard dislocations would introduce extra columns in the image, particularly in the center of the two-column doublets. However, we have not observed such an image.

V. CONCLUSIONS

Using Z-contrast imaging in the STEM, we have directly observed a large variety of dislocation cores distinct from the standard core structure. Three variations of dislocation cores were analyzed in detail. Two of the structures—the elongated and composite cores—contain extra 2×1 reconstructions. These "extensions" of the standard core structure may be a transition between edge dislocations and dissociated dislocations. The third structure—the transformed core—seems to have a chemical composition that is entirely different from $SrTiO_3$. It resembles a nanotube of TiO imbedded in a $SrTiO_3$ matrix. This large variation of dislocation structures opens

the door further to using grain boundary doping to influence grain boundary properties and, ultimately, the properties of the bulk material.

ACKNOWLEDGMENT

This work was supported by the United States Department of Energy Grant No. DE-FG02-03ER46057.

REFERENCES

1. J. Mannhart, P. Chaudhari, D. Dimos, C.C. Tsuei, and T.R. McGuire: Critical currents in [001] grains and across their tilt boundaries in $YBa_2Cu_3O_7$ films. *Phys. Rev. Lett.* **61,** 2476 (1988).
2. D. Dimos, P. Chaudhari, and J. Mannhart: Superconducting transport-properties of grain-boundaries in $YBa_3Cu_3O_7$ bicrystal. *Phys. Rev. B* **41,** 4038 (1990).
3. N.D. Mathur, G. Burnell, S.P. Isaac, T.J. Jackson, B.S. Teo, J.L. MacManus-Driscoll, L.F. Cohen, J.E. Evetts, and M.G. Blamire: Large low-field magnetoresistance in $La_{0.7}Ca_{0.3}MnO_3$ induced by artificial grain boundaries. *Nature* **387,** 266 (1997).
4. N. Zhang, W.P. Ding, W. Zhong, D.Y. Xing, and Y.W. Du: Tunnel-type giant magnetoresistance in the granular perovskite $La_{0.85}Sr_{0.15}MnO_3$. *Phys. Rev. B: Condens. Matter* **56,** 8138 (1997).
5. W. Heywang: Resistivity anomaly in doped barium titanate. *J. Am. Ceram. Soc.* **47,** 484 (1964).
6. R.F. Klie, J.P. Buban, M. Varela, A. Franceschetti, C. Jooss, Y. Zhu, N.D. Browning, S.T. Pantelides, and S.J. Pennycook: Enhanced current transport at grain boundaries in high-T_C superconductors. *Nature* **435,** 475 (2005).
7. J.P. Buban, K. Matsunaga, J. Chen, N. Shibata, W.Y. Ching, T. Yamamoto, and Y. Ikuhara: Grain boundary strengthening in alumina by rare earth impurities. *Science* **311,** 212 (2006).
8. Y. Sato, J.P. Buban, T. Mizoguchi, N. Shibata, M. Yodogawa, T. Yamamoto, and Y. Ikuhara: Role of Pr segregation in acceptor-state formation at ZnO grain boundaries. *Phys. Rev. Lett.* **97,** 106802 (2006).
9. M. Kim, G. Duscher, N.D. Browning, K. Sohlberg, S.T. Pantelides, and S.J. Pennycook: Nonstoichiometry and the electrical activity of grain boundaries in $SrTiO_3$. *Phys. Rev. Lett.* **86,** 4056 (2001).
10. S.D. Mo, W.Y. Ching, M.F. Chisholm, and G. Duscher: Electronic structure of a grain-boundary model in $SrTiO_3$. *Phys. Rev. B: Condens. Matter* **60,** 2416 (1999).
11. M.M. McGibbon, N.D. Browning, M.F. Chisholm, A.J. Mcgibbon, S.J. Pennycook, V. Ravikumar, and V.P. Dravid: Direct determination of grain-boundary atomic-structure in $SrTiO_3$. *Science* **266,** 102 (1994).
12. V. Ravikumar, R.P. Rodrigues, and V.P. Dravid: An investigation of acceptor-doped grain boundaries in SrTiO3. *J. Phys. D: Appl. Phys.* **29,** 1799 (1996).
13. R.P. Rodrigues, H.J. Chang, D.E. Ellis, and V.P. Dravid: Electronic structure of pristine and solute-incorporated $SrTiO_3$: II, Grain-boundary geometry and acceptor doping. *J. Am. Ceram. Soc.* **82,** 2385 (1999).
14. N.D. Browning and S.J. Pennycook: Direct experimental determination of the atomic structure at internal interfaces. *J. Phys. D: Appl. Phys.* **29,** 1779 (1996).
15. G. Duscher, J.P. Buban, N.D. Browning, M.F. Chisholm, and S.J. Pennycook: The electronic structure of pristine and doped (100) tilt grain boundaries in $SrTiO_3$. *Interface Sci.* **8,** 199 (2000).
16. R.F. Klie and N.D. Browning: Atomic scale characterization of oxygen vacancy segregation at $SrTiO_3$ grain boundaries. *Appl. Phys. Lett.* **77,** 3737 (2000).
17. Z.L. Zhang, W. Sigle, W. Kurtz, and M. Ruhle: Electronic and atomic structure of a dissociated dislocation in $SrTiO_3$. *Phys. Rev. B: Condens. Matter* **66,** 094108 (2002).
18. Z.L. Zhang, W. Sigle, and M. Ruhle: Atomic and electronic characterization of the a[100] dislocation core in $SrTiO_3$. *Phys. Rev. B: Condens. Matter* **66,** 094108 (2002).
19. R. Astala and P.D. Bristowe: First-principles calculations of an oxygen deficient Sigma=3 (111) [10$\bar{1}$] grain boundary in strontium titanate. *J. Phys. Condens. Matter* **14,** 6455 (2002).
20. R.F. Klie, M. Beleggia, Y. Zhu, J.P. Buban, and N.D. Browning: Atomic-scale model of the grain boundary potential in perovskite oxides. *Phys. Rev. B: Condens. Matter* **68,** 214101 (2003).
21. S.Y. Choi, J.P. Buban, M. Nishi, H. Kageyama, N. Shibata, T. Yamamoto, S.J.L. Kang, and Y. Ikuhara: Dislocation structures of low-angle boundaries in Nb-doped $SrTiO_3$ bicrystals. *J. Mater. Sci.* **41,** 2621 (2006).
22. M. Varela, S.D. Findlay, A.R. Lupini, H.M. Christen, A.Y. Borisevich, N. Dellby, O.L. Krivanek, P.D. Nellist, M.P. Oxley, L.J. Allen, and S.J. Pennycook: Spectroscopic imaging of single atoms within a bulk solid. *Phys. Rev. Lett.* **92,** 095502 (2004).
23. A.P. Sutton and R.W. Ballurri: *Interfaces in Crystalline Materials* (Claredon Press, Oxford, 1995).
24. J.P. Buban, H. Iddir, and S. Ogut: Structural and electronic properties of oxygen vacancies in cubic and antiferrodistortive phases of $SrTiO_3$. *Phys. Rev. B: Condens. Matter* **69,** 180102 (2004).
25. M. Sankaraman and D. Perry: Valence determination of titanium and iron using electron-energy loss spectroscopy. *J. Mater. Sci.* **27,** 2731 (1992).
26. T. Mizoguchi, Y. Sato, J.P. Buban, K. Matsunaga, T. Yamamoto, and Y. Ikuhara: Sr vacancy segregation by heat treatment at $SrTiO_3$ grain boundary. *Appl. Phys. Lett.* **87,** 241920 (2005).
27. F.M.F. De Groot, J. Faber, J.J.M. Michiels, M.T. Czyzyk, M. Abbate, and J.C. Fuggle: Oxygen 1s x-ray-absorption of tetravalent titanium-oxides—A comparison with single-particle calculations. *Phys. Rev. B: Condens. Matter* **48,** 2074 (1993).
28. R. Brydson, H. Sauer, W. Engel, and F. Hofer: Electron energy-loss near-edge structures at the oxygen K-edges of titanium(IV) oxygen compounds. *J. Phys. Condens. Matter* **4,** 3429 (1992).
29. I. Tanaka, T. Nakajima, J. Kawai, H. Adachi, H. Gu, and M. Ruhle: Dopant-modified local chemical bonding at a grain boundary in $SrTiO_3$. *Philos. Mag. Lett.* **75,** 21 (1997).
30. C. Mitterbauer: Thesis, Graz University of Technology (2003).